

Small Aperture Pulsar Detection

Peter East

Introduction

It has long been believed that pulsar detection by amateurs is extremely difficult and that large antennas, complex receivers and difficult processing is required to achieve any success. Some amateurs have, however, piloted the way with quite modest systems and this article builds on their success. In it, the tools are shared that will enable an interested party to design their own system and process the data, to confidently detect the strongest pulsar in either the Earth's northern or southern hemispheres. The key parameters to success with minimum expenditure exploit the increasing pulsar flux levels at low frequencies, availability of software defined radios, easily constructed receiving antennas and freely available processing software. This article begins by examining the fundamental radiometer equation to demonstrate what system characteristics are important and discusses how best to choose the antenna and main receiver components to facilitate amateur pulsar detection. Finally some practical results are presented together with methods of validating detections.

The Pulsar Radiometer Equation

Equation 1 is the pulsar radiometer equation⁽¹⁾ which describes the best possible folding algorithm performance in generating an observable signal-to-noise ratio (SNR),

$$SNR = \frac{S_p A_e \sqrt{n_p t_{int} \Delta f}}{2 \beta k_b T_{sys}} \sqrt{\frac{P - W}{W}} \quad (1)$$

where, S_p is the pulsar mean total flux at the observation frequency, as listed in the ATNF data base (<https://www.atnf.csiro.au/research/pulsar/psrcat/>).

A_e is the receiving antenna effective collecting area in m^2 .

n_p is the number of polarizations received.

t_{int} is the total integration time in seconds.

Δf is the receiver RF bandwidth.

P is the pulsar period.

W is the pulsar half-height pulse width.

factor 2 halves the pulsar flux to conform with the flux with a single polarization.

β is a modifying factor to account for digitization losses for coarser digital increments.

k_b is Boltzmann's constant.

T_{sys} is the receiver system noise temperature.

Given the pulsar mean flux S_p , the key parameters are the effective receiving aperture, the integration time, the receiver RF bandwidth and of course the receiver system noise temperature. Making the assumptions that an amateur's system comprises a modern software defined radio (SDR) with computer processing fed by a small fixed antenna, then, when observing a pulsar in drift-scan mode over the antenna 3 dB beamwidth, this equation can be adapted to suit and becomes,

$$SNR = \frac{736 b S_p}{T_{sys}} \sqrt{\frac{\Delta f}{f}} \sqrt{r A_e^3} \sqrt{\frac{P - W}{W}} \quad (2)$$

where, b is the antenna beam shape integration loss factor (~ 0.8 for over a typical antenna 3 dB beamwidth).

f is the receiver RF center frequency and Δf the RF bandwidth, both in MHz.
 r is the antenna azimuth to elevation beamwidth ratio for elliptical beams.
 S_p is now measured in Jansky units and A_e , the antenna effective collecting area is in m^2 .

The RF frequency now becomes a factor due to the beamwidth for a given aperture being frequency dependant. So low frequencies give broader beamwidths and longer drift scan integration times. The increased pulsar flux at lower frequencies is another positive aspect. Figure 1 plots the expected SNR from fully folded data observed for the duration that the pulsar is illuminated within the antenna 3 dB beamwidth. Here, the antenna is assumed to have equal azimuth and elevation beamwidths; the RF frequency is 400 MHz, and SDR bandwidth 2.4 MHz (the RTL2832U SDR is assumed) and the system noise temperature is 100 °K. The dashed lines at the bottom of the plot show the expected folded noise peak level (SNR < 3). and also, a pulsar possible recognition level of SNR = 5.

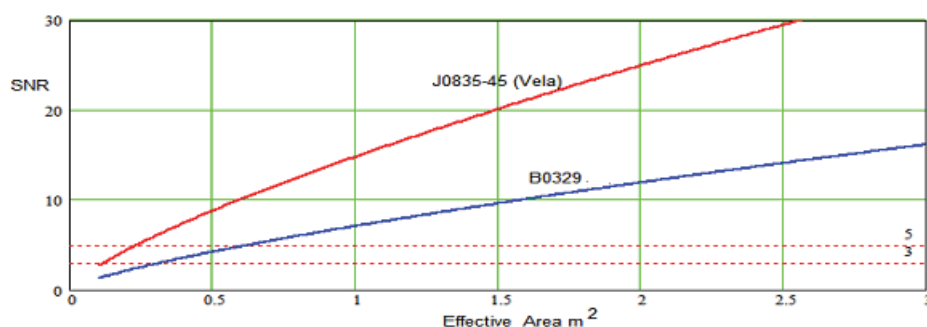


Figure 1. Equation 2 Drift-Scan Detection SNR for Vela and B0329+54 with $T_{\text{sys}} = 100$ °K at 400 MHz RF and 2.4 MHz RF Bandwidth.

The plots show that with a system noise temperature below 100 °K, at 400 MHz it should be possible to just detect the Vela pulsar (J0835-45) with receiving apertures down to 0.25 m^2 . For B0329 (B0329+54), pulsar receiving apertures exceeding 0.6 m^2 are required. These are of course ideal conditions; natural pulsar scintillation and local RF interference limits success in real trials.

The conclusions from these curves are that our southern hemisphere friends have an easier detection task, but more importantly, by aiming for a low system noise temperature, it is clearly possible for conveniently situated amateurs to confidently detect the two strongest known pulsars with small aperture antennas of the order 1 to 2 m^2 .

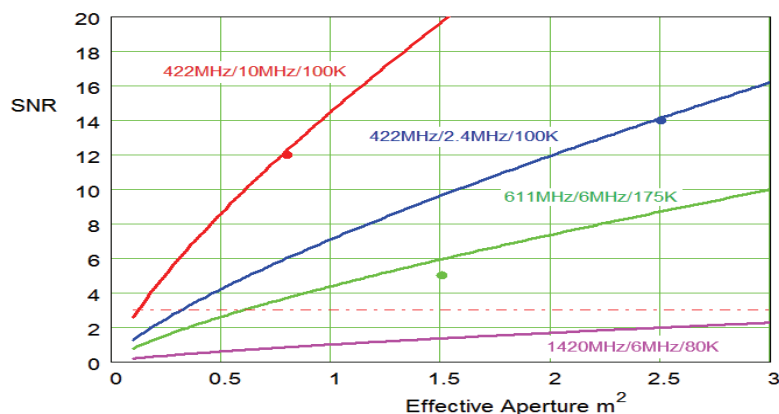


Figure 2. Drift Scan Detection Plots for Pulsar B0329 with Amateur Results

Figure 2 plots the theoretical detection/aperture curves for the B0329 pulsar at various frequencies noted together with dots plotting actual amateurs trial-average results^(6,10). The red and blue dot results were obtained with modest systems by Andrea Dell'Immagine⁽⁶⁾ in Italy. Different chosen RF frequencies (Figure 2) also modify the SNR plots since pulsar flux tends to reduce with higher frequency as does the antenna beamwidth for a constant aperture; for example at an RF of 1420 MHz the SNR figures drop by almost tenfold. The drop is caused partly by the pulsar flux drop but also because of the antenna beamwidth reduction for the same aperture and the consequent reduction in data gathering time in drift-scan mode.

Antenna Review and Issues

There are a variety of small antennas that can be considered for pulsar acquisition. Apart from effective aperture, the most important specification parameter is sidelobe performance. It is generally a feature of antennas with dimensions of a few wavelengths that their aperture efficiency is low due to energy lost in sidelobes.

Estimating Sidelobe Temperature

Assuming an antenna with 2 m² aperture at 400 MHz, the beamwidth can be expected to be around 28° and the directivity of the order 17 dB. A measured Yagi polar pattern with this specification is shown in Figure 4.

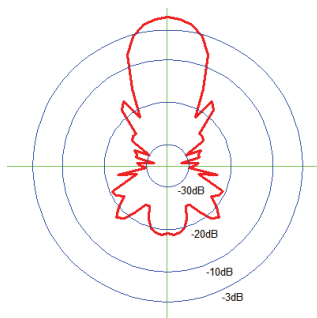


Figure 4. 28° Beamwidth Yagi Antenna Average E/H Polar Response

A very simple analysis assumes that in addition to the main beam, it can be imagined that in three dimensions there are a number of side and back lobes, averaging, say -20 dB (=1/100) through the remaining 4π steradian sphere, equivalent to 41253 square degrees.

The total sidelobe temperature can be estimated by imagining the antenna placed inside a container with the walls at ambient temperature of 290 degrees. Now we can see that the proportion of temperature seen by the main beam is $T_{mb} = 28^2 \times 290$ and in the sidelobes $T_{sl} = (41253 - 28^2) \times 290 / 100$. From these identities we can deduce the aperture efficiency as $T_{mb} / (T_{sl} + T_{mb}) = 66\%$ and the total sidelobe temperature $(1 - 0.66) \times 290 = 98.6^\circ$.

In use, placing the antenna pointing directly upwards on the ground, then up to half the sidelobes can illuminate the ground at a temperature of 290° and so could contribute about 50° to the receiver system noise temperature (effectively raising a 0.4dB LNA noise figure to ~1dB). Indeed if the site is such that the local horizon, due to trees, buildings etc., is at an elevation of 30°, the system noise temperature could be increased by more than 70° K.

Antenna Choices

Without a doubt, a large parabolic dish is the obvious solution but the cost, size, installation, drive requirements and space required may put it outside the scope of the average amateur. A smaller off-set satellite dish upwards of 1.5 m is a strong contender, however at 400 MHz, illumination efficiency and blockage can still cause efficiency problems.

Yagi⁽²⁾ and helical antennas for this frequency band need to be quite long (>5 wavelengths, λ) to provide sufficient effective area; but as stated above do not have very good side and back-

lobe performance. These antenna types can be arrayed linearly to advantage by ensuring that the integration time is controlled by the basic element beamwidth and not by the array length. Yagis have a weight and physical cross-section advantage; for example a 17-element Yagi has a gain around 16 dB, a length (L) of 5 wavelengths and an effective area of $3 \lambda^2$. For long Yagis, a useful guide to the effective aperture is the relation, $A_e \approx 0.6L\lambda$. Horn⁽³⁾ antennas have lower side- and back-lobes with less effect on system noise temperature. At 400 MHz they are a bit bulky, possibly demanding a length of at least 2 m and aperture 1.4 m x 1.4 m but they can be manufactured with lightweight aluminium clad materials.

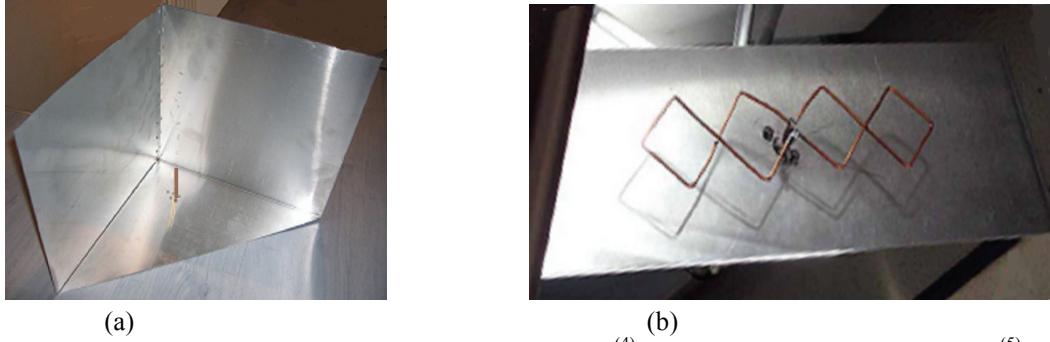


Figure 5. (a) 3D Corner Reflector Antenna⁽⁴⁾ and (b) Double Bi-Quad Antenna⁽⁵⁾

The 3D-corner reflector and double bi-quad antennas (Figure 5) have both demonstrated excellent performance⁽⁶⁾ for pulsar work. Aluminium sheet constructions are shown in Figure 5 although lighter wire mesh reflectors are also practical providing the mesh apertures are less than about $\lambda/20$. They exhibit very low back-lobes so the basic receiver system noise temperature is less affected. However, these designs have the property that they are gain limited - that means that their maximum apertures are wavelength-limited ($\sim 5 \lambda^2$ for the 3D corner reflector and about $1.7 \lambda^2$ for the double bi-quad), so for pulsar detection, they work best at lower frequencies where they have a useful physical collecting area. When optimally oriented, the azimuth/elevation beamwidth factor r in Equations 2 is 1.5 and 1.7 for the 3D and double bi-quad antennas respectively. The latter figure assumes the bi-quads are aligned linearly towards the source. The 3D corner reflector antenna beam pointing direction is at 45° relative to the base plane. Another possible antenna for this application to fill the small aperture parabolic dish gap is the backfire antenna^(7,8). The standard and short backfire antennas achieve high aperture efficiency and low sidelobes in the frequency and aperture ranges considered here.

Receiver Implementations

Figure 6 schematic shows a basic pulsar radio telescope setup.

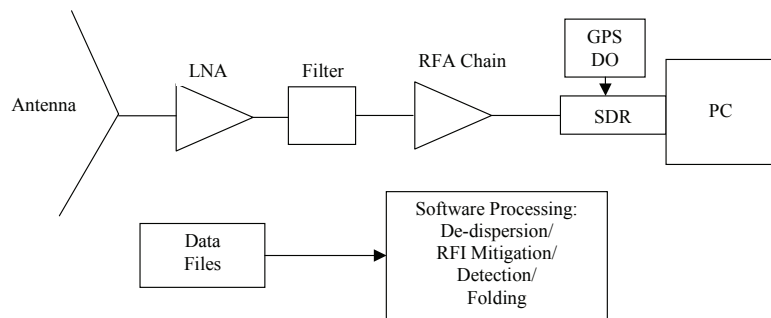


Figure 6. Basic Pulsar Radio Telescope

The key pre-requisites for a successful B0329 pulsar receiving system are;

1. Low RFI 300/400/600MHz band choice.
2. Antenna aperture, $>1.5 \text{ m}^2$.
3. LNA noise figure $< 0.5 \text{ dB}$ + good band-pass filtering.
4. SDR bandwidth $>2\text{MHz}$, tuning accuracy $<0.5\text{ppm}$ or GPS disciplined oscillator locked.
5. PC/laptop, $>2\text{GHz}$ clock, $>200\text{GB}$ storage free, Windows/Linux 64B OS.

Requirements 1, 3 and 4 are discussed in detail below.

1. Radio Frequency Interference

RFI comprises any non-pulsar electromagnetic signal within the observation frequency band. In fact, large saturating signals outside the operating band but within the LNA band, can cause within-band noise modulations that may impact on the folded pulsar result. Some LNAs are available with pre-filtering but a good post-LNA band-defining filter with $>50 \text{ dB}$ out of band rejection is essential. Amplitude modulated signals, digital transmissions, cell phones, TV, transient signals such as motor ignition, electric hand tools, solar power panels, PC digital clocks, can have a serious impact on the folded result. Experience has shown that nighttime/early morning observations suffer less than daytime runs. Prior to choosing the astro-band for operation, freely available spectrum analysis software (SDR Sharp etc.) is useful for comparing band RFI activity but it is important to realize that the pulsar signals are several tens of dB below the noise/RFI levels observed in this way.

To minimize false reports or SNR degradation, RFI mitigation techniques may need to be applied prior to folding. Since interference may be sporadic, it is usual to sense RFI in the recorded data and blank bad data sections in both frequency and time. The PRESTO software has easy-to-use tools embedded to remove RFI in both frequency and time domains. In the first instance, it is recommended that effort is concentrated on identifying a low RFI band and carry out observations in the early hours - at the right time of the year, of course.

3. Receiver components

LNA noise figures below 0.4 dB are desirable; several are available based on the EpHEMT GaAs technology. A commercial Mini-Circuits LNA, the ZX60-P33ULN, has a 0.4 dB noise figure (400 - 1400 MHz) contributing 28° to the system noise temperature.



Figure 7. Low-Noise Amplifiers - left from Mini-Circuits, right from ebay

As shown in Figure 7, a benefit from the mobile phone industry, cheap LNAs are advertised on ebay, although not so highly specified as the commercial amplifiers, they may still be suitable for later RF chain amplification. Even lower noise narrow-band amplifiers are available from radio amateur enthusiasts, driven by the Earth-Moon-Earth (EME) communication specialists. RF filtering is necessary to prevent digital TV and other commercial radio stations from over-driving the RF amplifiers into saturation. However, since LNAs are fairly low gain ($\sim 20\text{dB}$) overdriving of the first LNA in quiet environments is unusual but pre-RF chain filtering is probably essential. A suitable band-pass interdigital filter (Figure 8) can be designed using the online tool⁽⁹⁾ by A. Changpuak.

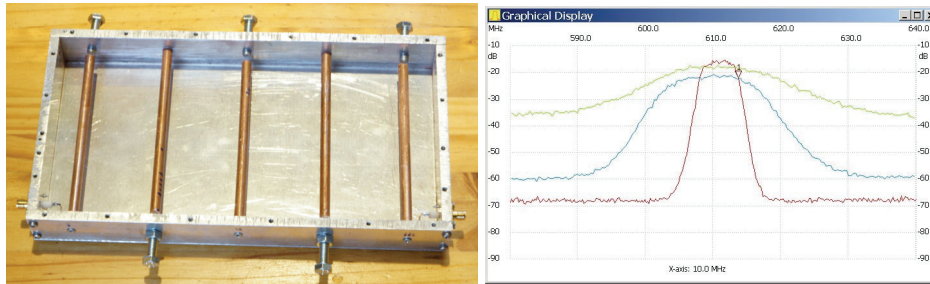


Figure 8. 611 MHz, 5-element Interdigital Filter and Tuned Response (red)

Receiver Design Considerations

Ideally, the LNA should define the system sensitivity, but there are several system demons that conspire to degrade it. Resistive losses in the antenna LNA input path both increases system noise and reduce wanted signal/noise amplitude and are to be avoided. Cable mismatch reduces the wanted signal so that good LNA input and antenna terminal matching is important for maximum power transfer. Antenna sidelobe ground noise has been discussed earlier, coupled with unwanted RFI, the result can be catastrophic. There are however steps that should be followed to mitigate these degradations such as, placing the LNA as near to the antenna terminal as possible, choosing a low sidelobe antenna type and ensuring the antenna, is as well-matched to the standard $50\ \Omega$ as possible. There are cheap antenna vector analyzers available on ebay suitable for this purpose.

Free SDR software such as SDR Sharp is useful for measuring the detected noise level proportional to $T_{LNA} + T_{load}$ with the load connected and T_{LNA} with the input open-circuited. Comparing these levels with that when the antenna is connected ($T_{LNA} + T_{Ant}$), enables a coarse indication of the working system noise temperature.

4. SDR Receivers

There are a number of software defined radios (SDRs) on the market with various capabilities and software support. The cheapest by far is the RTL2832U unit, originally intended for digital TV but interested engineers developed drivers and software for it to become a useful 2.4 MHz bandwidth tunable SDR. The basic unit frequency and temperature stability is not good, but both characteristics can be adequately improved with crystal modifications and additional cooling. Multiple RTLs can be frequency locked together⁽¹⁰⁾ to cover broader RF bandwidths, but better wider band SDRs, such the Airspy, have been used successfully.



Figure 9. RTL2832U SDR

The RTL frequency setting accuracy can be improved by replacing the on-board crystal with an external 0.5 ppm temperature controlled crystal oscillator (TCXO). A better, and not too expensive alternative, is to use a SDR-Kits GPS disciplined oscillator tuned to 28.8 MHz to drive the RTL via a CMOS inverter⁽¹⁰⁾. Now with an SDR tuning accuracy of the order of 1 part per billion and an accurate prediction of the topocentric period, it should not now be necessary to tune the folding period setting to search for the pulsar response.

Software Resources

There are several SDR software graphical packages such as SDR Sharp that are compatible with the RTL SDR and other SDRs that are very useful for system commissioning and testing and in some cases to produce data files. But for real time data collection, the software tools of Osmocom⁽¹¹⁾ are essential. For data processing several amateurs have developed bespoke software for synchronous detection and data display and have made these available:-

Software Source Summary

Testing:	SDR# + Zadig Driver; from: <i>airspy.com</i>
Data Recording:	Osmocom rtl tools: <i>rtl_sdr.exe</i> from: <i>sdr.osmocom.org</i> GnuRadio - internet download
Processing:	<i>dedispers22co.exe</i> , <i>rapulsar22conv.exe</i> from: <i>ylpwe.co.uk/RAProgs</i> 3pt analysis tools from: M Klaassen: <i>parac.eu</i>
Display:	Excel/MathCad/MatLab/PRESTO
Programming:	Anaconda3 - internet download
Professional Analysis:	TEMPO, PRESTO, SigProc (Linux) from: <i>pulsarastronomy.net</i>
Ephemeris Data:	Radio-Eyes from: <i>radiosky.com</i>
Pulsar Timing:	Accurate prediction of the pulsar topocentric period at the antenna latitude/ longitude and acquisition UTC. TEMPO or on-line calculators.

Acquisition and Processing Software

Basic Approach

Amateur data collection and processing software for the RTL SDR in 'MS Windows' is described and links are shared in Reference 10. The software pulsar processing sequence of Reference 10 is outlined in Figure 10. These are run in Windows/DOS command terminal windows and resulting text data files can be viewed in Excel or MathCad/MatLab programs

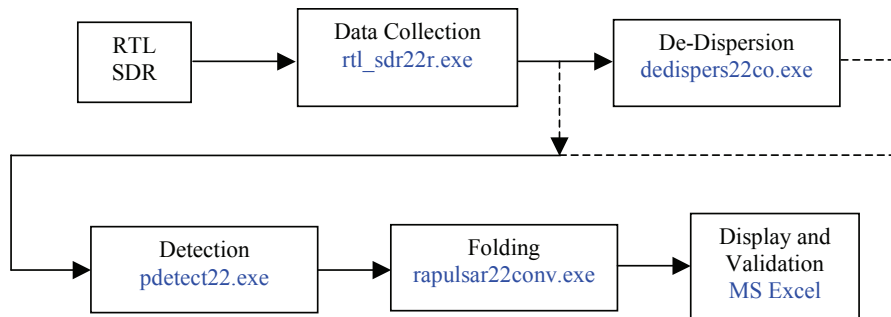


Figure 10. Data Acquisition and Processing Sequence

Amateur Small Aperture Results

The most successful amateur pioneer of small aperture pulsar detection is Andrea Dell'Immagine from Italy. For some years, he ran an online radio telescope monitoring the B0329+54 pulsar (<http://iw5bhy.altervista.org>) on a daily basis. His 3D corner reflector antenna, tuned to 422MHz, driving a 2.4MHz clocked RTL2832U and a typical 3 hour recording result is shown in Figure 11, He has also demonstrated viability of B0329 detection using a 0.8 m² double bi-quad antenna at 422 MHz driving a 10 MHz Airspy SDR. His achieved results are indicated by the red and blue spots in Figure 2.

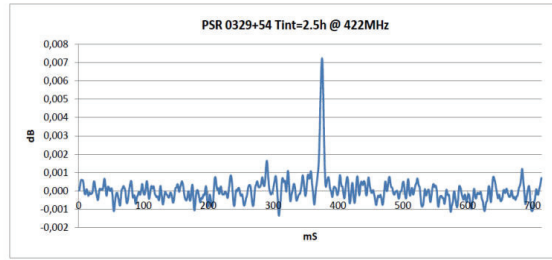


Figure 11. A Dell'Immagine's Radio Telescope and Typical 15:1 SNR Pulsar Record.

The author's later, less capable effort using twin 2.5m Yagis at 611 MHz and a triple RTL (609,611,613 MHz) receiver⁽¹⁰⁾ to compensate is illustrated below in Figure 12.

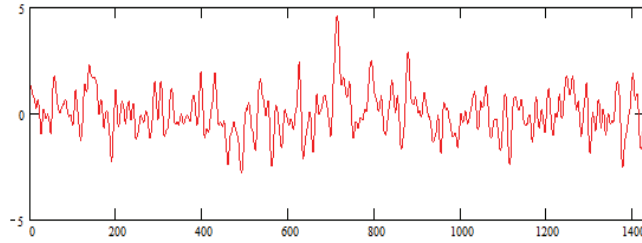


Figure 12. Author's Radio Telescope and Typical 4.5:1 SNR Pulsar Record.

Pulsar Detection Validation

For strong pulsar signals where the acquired signal-to-noise ratio is greater than 10:1, the successful event may be obvious, but the application to the PRESTO analysis software is confirmation. The Presto results for Figures 11 and 12 are presented in Figure 13.

Comparing the two plots in Figure 13, attention is drawn to the upper left pulse displays. It is clear that the left hand plot SNR is superior.

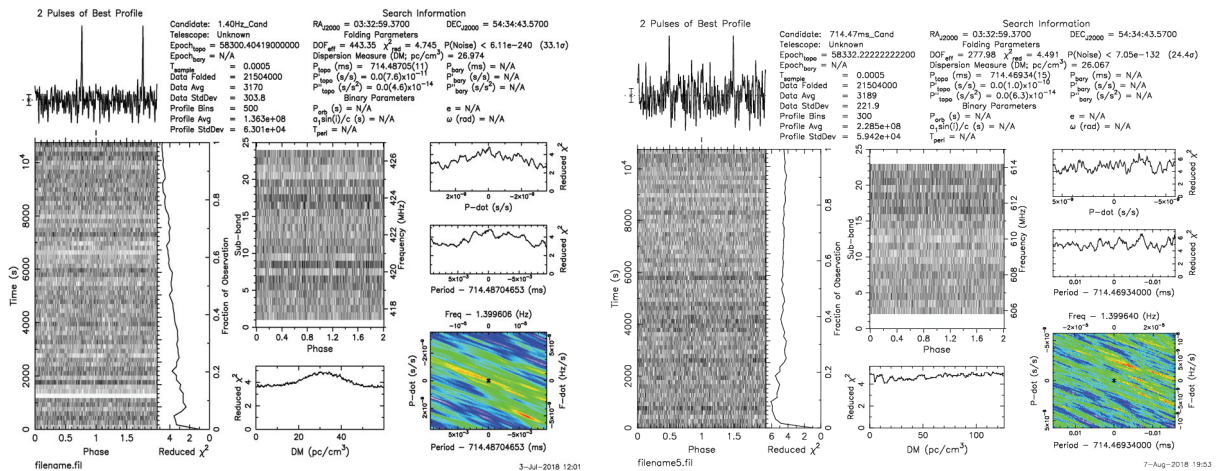


Figure 13. PRESTO Plots for the Systems of Figure 11 (left) and 12 (right).

The center bottom plot on the left represents a dispersion search plot and again it is clear that the left-hand plot shows a nice peak around the expected Dispersion Measure value of 26.7 but the right-hand plot with the low SNR, the DM is indeterminate. Finally, the colored plot bottom right shows a red peak in the center, a measure of the correct period and period rate (P-dot) searches, again indeterminate in the right hand plot.

It is clear from this comparison that for weaker SNRs, it is necessary to study the data further. For this an 8-point validation process has been proposed which exploits common pulsar characteristics to differentiate candidate pulsar peaks from the underlying folded random noise/interference. The recommended checking sequence⁽¹²⁾ is;

1. Maximum occurs at the correct topocentric period
2. Correct pulse width
3. Multi-section fold correlation
4. Multi-period fold correlation.
5. Multi-band correlation.
6. Period search peak – match profile, offset and pulse width
7. P-dot search peak – match profile, offset and pulse width
8. Dispersion search peak – amplitude and pulse width

The validation checks are necessary because the noise peaks in the final fold arise for a similar reason that the pulsar does. The folding of some thousands of data periods picks out noise features that occur in a dominant number of periods - and conversely true pulsar pulses may not be significant in all data periods. The pulsar candidate must pass all these tests. For moderate SNRs (>6) these tests are strong indicators, but for SNRs <4 , much more care may be needed. These validation tests, their underlying characteristics and theory supporting their use is detailed in Reference 12. Once positively identified, daily records can be added to provide improved SNR and indication of pulse detail.

Example Results - RT System, Figure 12

In small aperture pulsar detection systems, even very long-time data records may only produce detected SNR's of maybe only 2 to 5:1. Since the expected range of Gaussian noise peaks is in this region, there will always be some ambiguity in identifying a true pulsar pulse. Therefore, an extreme validation routine is necessary. Folded noise and unfortunate interference peaks can masquerade as pulsar-like signals and are a source of erroneous detections. All of the tests described can fall foul of noise/interference impersonations and pulsars themselves at this level do not have a 100% discriminating property. Initially, a preliminary check on data quality for acceptable RFI on downsampled amplitude-detected data should be made, then, band data aligned, bands de-dispersed, combined and initial drift, RF spikes etc: removed or nulled as described in the 'Processing Software' section above.

Validation Test 1 and 2

The combined file can then be inspected by running the folding software using the acquisition time's topocentric period ± 0.5 ppm at the receiver location.

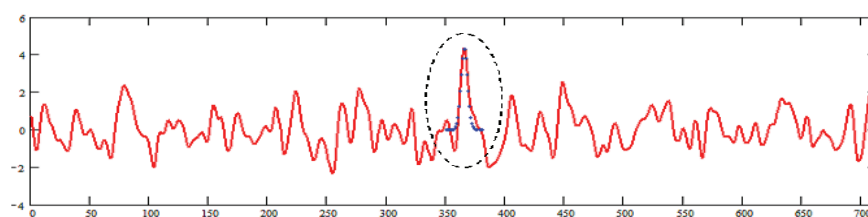


Figure 14. Matched-period fold (red) with pulse width Gaussian 6.5 ms pulse comparison (blue dots).
Data Record from System Figure 12 (T35_16:10:2017_01:53:00)

If a pulsar is present then a correlating pulse will appear in the folded result at an arbitrary phase and match the expected pulse width. (Figure 14).

Test 3

Figure 15 shows the result of folding the first and second halves of the data file and comparing them. It is clear that a positive indication in both halves occurs at the same phase as Figure 14. However, it is noticed that there are other similar correlations so this test whilst positive is not conclusive.

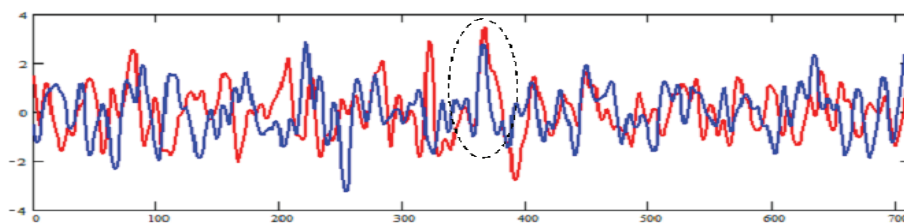


Figure 15. First half file (red) v second half (blue) file correlation

Test 4

Figure 16 shows the twin-period fold response of the data file, again showing strong correlation and pulsar pulse presence at the expected central bin. For this double-period folded presentation, the second pulse period has been overlaid on the first to illustrate central bin pulse coincidence.

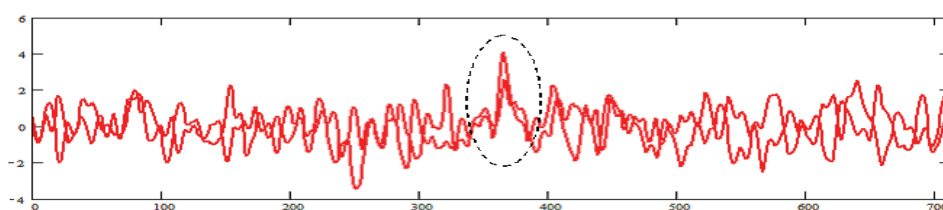


Figure 16. Double period fold and overlap.

Note again that this test is not conclusive as whilst the base noise waveform differs from Test 3, there are still common 'false' correlations.

Test 5

Figure 17 plots the correlation between three sub-bands folded individually but de-dispersed correctly and shows a positive correlation of the three separate band responses at the expected central bin. This test is quite strong, as being different frequency bands, the base noise must be uncorrelated and allowing for different scintillation effects, the pulsar is still expected to appear in all bands. There is of course, still a random probability of coincidence. Data for this plot was derived from a triple RTL2832U receiver solution but a similar result could be observed by splitting the spectrum of an alternative wideband SDR system.

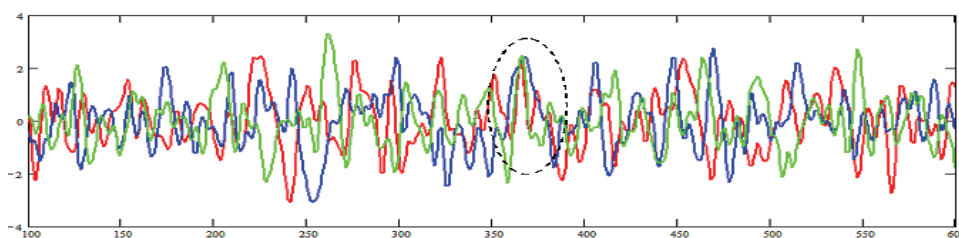


Figure 17. Band-to-band Correlation, red: 609 MHz , blue: 611 MHz, green: 613 MHz.

Tests 6 and 7

Figure 18 shows the effect of a period search. For this plot, the fold period has been adjusted by -1ppm (parts per million) for each plot, from the red curve to the magenta curve. The test is usually to find the peak matching fold period to confirm the correct fold period (red plot). However, it is noticed that as well as a predictable mean amplitude variation, there is also a predictable position shift. This can be shown to be equal to $-pT/2$, where p is the value of the period change in ppm and T is the total duration of the data record.

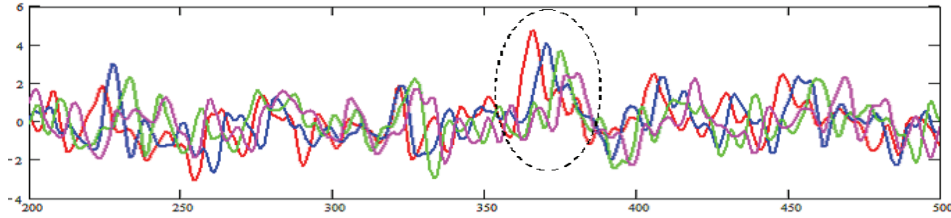


Figure 18. Period Search Plot (blue, -1ppm, green, -2ppm; magenta, -3ppm)

This appears a stronger test, as although, only negative ppm shift are shown for clarity, in this case, only the central pulsar candidate exhibits the expected characteristics. For a pulsar to conform to this test, despite scintillation it is a prerequisite that a pulsar pulse is present in the majority of periods. Random noise and RFI have less probability of passing this test. P-dot search is similar to the period search method, except that the search period is gradually increased during the data folding process. The result has similarities with period search but its peak shift detail is not so open to simple analysis and prediction checking.

Test 8

The dispersion property of pulsar signals is considered a primary identifier and adds maximum weight in verification. In this section, dispersion variation is defined as the frequency delay across the band (D) divided by pulse width (PW). The effects of positive or negative extra-dispersion on a pulsar pulse begin to be noticed when the magnitude of the total dispersion in ms across the band approaches the pulsar pulse width. At this point, the dispersed pulse width slightly increases and the amplitude drops by 15-20%. For larger dispersion delays, the pulse width increases to equal the delay. The amplitude drops by 50% when the band dispersion equals twice the pulse width ($D/W = 2$).

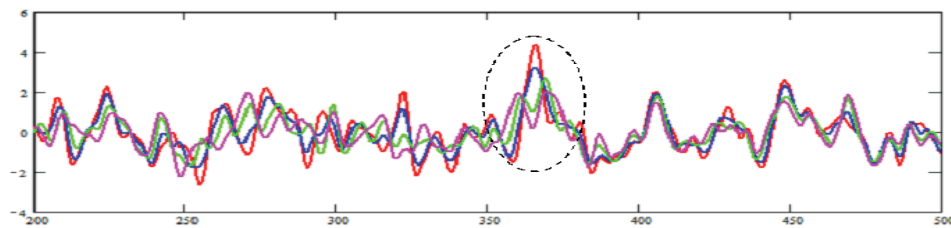


Figure 19. Dispersion Plot: $D/W = 0$ (red), ± 1 (blue), ± 2 (green), ± 3 (magenta)

Note in Figure 19 that whilst the amplitude and width changes on the central pulse candidate are still obvious, noise adds some distortion at low SNR. Noise peaks are largely unaffected.

Pulsar Correlation Recognition Algorithm

Based on the observation from Figure 15 that splitting the data record in two halves somewhat de-correlates the noise base, the technique here exploits this to improve pulsar visibility. Noise de-correlation also occurs between the folded periods when two period folding (Figure 16). Cross-correlating the positive excursions of the split fold results from both methods enhances recognition of potential repetitive pulsar candidates to ease low SNR pulsar recognition.

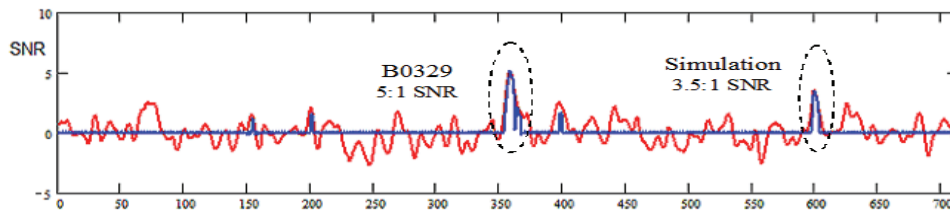


Figure 20. 5:1 SNR Pulsar + 3.5:1 SNR Simulation (red) - Correlation Result in blue

Figure 20 shows the result of cross-correlating multiple split folds. It achieves better pulsar and simulation pulse visibility by taking advantage of randomizing the positions of discrete periods in the data record before combining multiple split correlations. The blue plot in Figure 20 results from correlating 50 randomizations and shows that most of the noise peaks have been voided whilst the pulsar and simulation are preserved. This result might be expected by observing that adding each pair of randomized half-folds must always result in the standard red plot full-fold.

Challenges and Conclusions

The key conclusions that are drawn from this article are,

1. Pulsars Vela in the Southern hemisphere and B0329+54 in the Northern hemisphere can be detected in the 300/400/600Mhz radio astronomy-allocated RF bands using home-made, small aperture ($<2\text{m}^2$) antennas, providing local RFI is not too severe.
2. There is a choice of antenna types but the main antenna design requirement is for low side and back lobes and preferably operated in a site with a clear, open horizon.
3. Understanding pulsar pulse train properties is key to identifying low SNR pulsars in RFI and noise.

There remain challenges however; the pulsar signal scintillates over both frequency and time so the integrated signal amplitude varies sometimes considerably, so not all trials may be successful. Additionally there may be local sporadic RF interference, which, unless it is easily mitigated by blocking bad frequency and time data sections, then wanted pulsar signals may be obscured, again leading to trials results variability. The PRESTO software running on Linux is particularly good at ensuring only good data is folded and is worth trying. Finally, there is the problem of validating weak signals but with experience, confident identification of data SNRs close to noise peaks is possible.

References

- [1] D Lorimer, M Kramer. Handbook of Pulsar Astronomy. Cambridge University Press, 2005.
- [2] P McMahon, VK3DIP. Yagi Design Calculator, <https://www.yagicad.com/>
- [3] Horn Antenna Calculator. <https://hornantennacalculator.blogspot.com/p/calculator.html>
- [4] D Dobrić YU1AW. 3D Corner Reflector Antenna, https://qsl.net/yu1aw/ANT_VHF/Shortened%203D%20Corner%20Reflector%20Antenna.pdf
- [5] J Steelman. Double Bi-Quad Antenna Calculator, <https://jeroen.steeman.org/Antenna/double-biquad-antenna>
- [6] A Dell'Immagine, IW5BHY. Italian Amateur Radio Station. <http://iw5bhy.altervista.org/info.php>
- [7] LR Dod. Backfire Yagi Antenna Measurements, <https://ntrs.nasa.gov/archive/nasa/casi.ntrs.nasa.gov/19680012807.pdf>
- [8] G. S. Kirov, H. D. Hristov. Study of Backfire Antennas, www.scielo.br/pdf/jmoa/v10n1/01.pdf
- [9] Changpuak. Interdigital Bandpass Filter Designer http://www.changpuak.ch/electronics/interdigital_bandpass_filter_designer.php
- [10] PW East, A Minimal Pulsar Detection System. Journal of the Society of Amateur Radio Astronomers. January-February 2018. p36. <http://www.y1pwe.co.uk/RAProgs/MiniPulsarRx.pdf>
- [11] Osmocom RTL-R Site, <https://osmocom.org/projects/rtl-sdr/wiki/Rtl-sdr>
- [12] PW East. An Analytical Method of Recognizing Pulsars at Moderate SNR. Journal of the Society of Amateur Radio Astronomers. November-December 2018. p17. <http://www.y1pwe.co.uk/RAProgs/Pulsars.html/PulsarAnalysisSNR2.doc>